CHALMERS
UNIVERSITY OF TECHNOLOGY

Near-field RIS-aided Localization under Channel Non-Stationarity: A Mismatched Model Approach

Citation for the original published paper (version of record):
Sun, B., Keskin, M., Rahal, M. et al (2024). Near-field RIS-aided Localization under Channel Non-Stationarity: A Mismatched Model Approach. IEEE Workshop on Signal Processing Advances in Wireless Communications, SPAWC: 271-275.
http://dx.doi.org/10.1109/SPAWC60668.2024.10694423

(article starts on next page)

Near-field RIS-aided Localization Under Channel Non-Stationarity: A Mismatched Model Approach

Bo Sun*, Musa Furkan Keskin‡, Moustafa Rahal†, Hui Chen‡, Jukka Talvitie*,
Henk Wymeersch‡, and Mikko Valkama*
*Faculty of Information Technology and Communication Sciences, Tampere University, Finland
†Institute for Communication Systems, 5G and 6G Innovation Centres, University of Surrey, United Kingdom
‡Department of Electrical Engineering, Chalmers University of Technology, Sweden
Email: {bo.sun, jukka.talvitie, mikko.valkama}@tuni.fi, m.rahal@surrey.ac.uk, {furkan, hui.chen, henkw}@chalmers.se

***Abstract*—With the increasing carrier frequencies and reconfigurable intelligent surface (RIS) apertures in future sixth-generation (6G) communication systems, the near-field region expands, causing more pronounced wavefront curvature and channel non-stationarity. By exploiting wavefront curvature-enabled localization with passive RIS, we propose a virtual sub-RIS-based channel model to approximate the true RIS channel. Based on this mismatched model, we propose and evaluate an iterative solution for localizing a user using narrowband pilots. Our numerical results at 28 GHz demonstrate clearly improved performance compared to the state-of-the-art reference method.**

***Index Terms*—Reconfigurable Intelligent Surfaces (RISs), mmWave Communication, Localization, Near-Field, 6G**

I. Introduction

With the worldwide commercial use of 5G technologies, researchers have shifted their focus to beyond fifth generation (B5G) and sixth-generation (6G) networks to meet more stringent requirements for future applications, such as extended reality [1]. Millimeter-wave (mmWave) and terahertz (THz) communications support the demands for throughput, latency, and localization accuracy but also suffer from severe propagation attenuation [2], [3]. Under these circumstances, reconfigurable intelligent surfaces (RISs) have been proposed to modify the propagation channel, thereby enhancing communication quality, extending coverage, and enabling localization functionality [4]–[6]. Moreover, with the increased carrier frequencies, future wireless systems will likely operate in the radiating near-field region, where the received signal on the RISs is subject to wavefront curvature [7], [8].

Recent research has intensively explored RIS-aided near-field localization, investigating various aspects of this technology, see, e.g. [9]–[15], considering both hybrid and passive RIS. Hybrid RISs have radio frequency (RF) chains to locally sense the channel state at the RIS, based on which two compressed sensing (CS) based estimation solutions using hybrid RIS are proposed in [9] and [10]. However, extra RF chains and information exchange increase system cost and overhead, leading to scalability challenges. To tackle the localization problem with passive RIS, [11] proposed a RIS profile optimization methods that enhance the localization accuracy, based on the user's coarse location information. In [12], the RIS phase profile was optimized and a near-field user localization method was proposed. In contrast, [13] extracted location information by exploring the covariance matrix of the RIS path's channel state information. However, all these methods fail to consider channel non-stationarity and instead employ a constant amplitude model for all RIS elements. To address this, [14] assumes the perfect knowledge of channel gains and coarsely estimates the user's location by exploring the received signal strength (RSS) in the region of interest, and then the iteration and weighted least-squares methods are used to refine the estimation, accounting for the channel non-stationarity. In [15], the whole RIS was broken down into tiles so that each tile experiences a predictable constant channel gain and then performs the maximum likelihood and time-difference-of-arrival (TDoA)-based localization solutions. These methods, however, depend heavily on the alignment between theoretical assumptions and practical channel conditions, with any mismatch leading to errors.

In this paper, we propose a localization method for passive RISs, accounting for both wavefront curvature and channel-

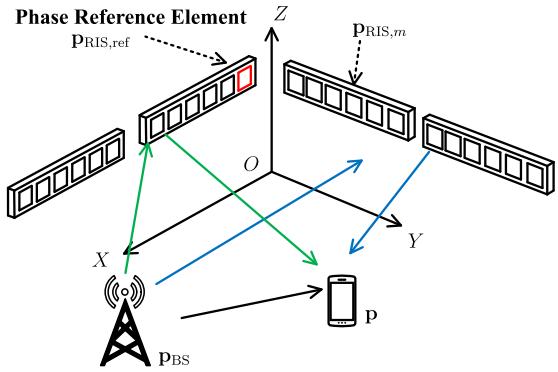

Fig. 1. Illustration of the considered SISO communication scenario involving a UE and a BS, located at locations $\mathbf{p}_{\text{BS}}$ and $\mathbf{p}$, respectively. A large multi-panel RIS is shown, and elements within each RIS panel are evenly and horizontally deployed on the walls. The location of the m-th RIS element in the Cartesian system is denoted as $\mathbf{p}_{\text{RIS},m}$, and the red color marked element serves as the reference point for computing the RIS steering vector.

This work has been supported by Business Finland under the 6G-ISAC project, the SNS JU project 6G-DISAC under the EU's Horizon Europe research and innovation Program under Grant Agreement No 101139130, and the Swedish Research Council (VR grant 2022-03007). This work has also been partially supported by the Research Council of Finland under the grants #352754, #357730, and #359095, and by the China Scholarship Council through Grant No 202107960017.

nonstationarity, without requiring a physical decomposition of the RIS and knowledge of channel amplitudes. Our study comprises the following key contributions: (i) We propose a flexible mismatched sub-RISs model and use it to approximate the true channel non-stationarity of the RIS link. (ii) We derive an iterative estimator for localizing the user and estimating the nonuniform channel amplitude, based on the flexible mismatched model. (iii) To assess the performance of our proposed estimators, we evaluate their root mean square error (RMSE) and establish a position error bound (PEB) using the proposed model. These evaluations demonstrate the effectiveness of the proposed work, compared to the state of the art.

Notations: Vectors and matrices are denoted by lowercase and uppercase bold letters, respectively. Vector elements are represented as $[\mathbf{a}]_m$. Sub-matrix of $\mathbf{J}$ from i-th to j-th rows and k-th to l-th colums is denoted by $[\mathbf{J}]_{[i:j,k:l]}$. Operators for Hermitian, transpose, pseudo-inverse and conjugation are $(\cdot)^H$, $(\cdot)^T$, $(\cdot)^\dagger$, and $(\cdot)^*$, respectively. The L2 norm is $\|\cdot\|$ and the argument of a complex number is $\arg(\cdot)$. $\Re\{\beta\}$ extracts the real components of complex input β. Moreover, the operator $\mathrm{Tr}(\mathbf{X})$ denotes the trace of matrix $\mathbf{X}$.

II. System Model and Problem Formulation

A. Geometry

We consider a 3D scenario where one base station (BS) acts as a transmitter and one user equipment (UE) as a receiver, while multiple phase-coherent RIS panels, acting as a large RIS with M elements, reflect the signal from BS to UE (see Fig. 1). BS and UE are equipped with an omnidirectional antenna. The RIS elements have a square shape with a length equal to a quarter of the carrier's wavelength, λ_c. Within every panel, element spacing is $\lambda_c/2$. The m-th element gain in incoming and reflecting orientations are $G_{\mathrm{i},m}$ and $G_{\mathrm{r},m}$, respectively.[1] In this Cartesian system, we present $\mathbf{p}_{\mathrm{BS}} = [x_{\mathrm{BS}}, y_{\mathrm{BS}}, z_{\mathrm{BS}}]^\top \in \mathbb{R}^{3\times 1}$ as a vector specifying BS's location. Likewise, the location of the m-th RIS element and the UE are expressed as $\mathbf{p}_{\mathrm{RIS},m} = [x_{\mathrm{RIS},m}, y_{\mathrm{RIS},m}, z_{\mathrm{RIS},m}]^\top \in \mathbb{R}^{3\times 1}$ and $\mathbf{p} = [x_{\mathrm{UE}}, y_{\mathrm{UE}}, z_{\mathrm{UE}}]^\top \in \mathbb{R}^{3\times 1}$, respectively.

B. Signal and Channel Model

Assuming a narrowband transmission model, the BS transmits constant amplitude pilot symbol $s_t \in \mathbb{C}$ to UE at instant $t \in \{0, 1, \ldots, 2T-1\}$ with the bandwidth W and transmit power $P_t = WE_s$. The corresponding received signal at UE is given by

$$y_t = (h_{\mathrm{LoS}} + h_{\mathrm{mp}} + h_{\mathrm{RIS},t})s_t + n_t, \tag{1}$$

where $n_t \in \mathbb{C}$ is independent identically distributed (i.i.d) complex Gaussian noise with zero mean and variance N_0. The channel models of the line-of-sight (LoS) path, multipath[2], and the RIS path are described by

$$h_{\mathrm{LoS}} = \alpha_0 e^{j\psi} e^{-j\frac{2\pi}{\lambda_c}(\|\mathbf{p}-\mathbf{p}_{\mathrm{BS}}\|)}, \tag{2}$$

$$h_{\mathrm{mp}} = e^{j\psi} \sum_{l=1}^{L} \alpha_l e^{-j\frac{2\pi d_l}{\lambda_c}}, \tag{3}$$

$$h_{\mathrm{RIS},t} = e^{j\psi} \mathbf{a}^\top(\mathbf{p}_{\mathrm{BS}}) \mathrm{diag}(\boldsymbol{\beta} \odot \boldsymbol{\omega}_t) \mathbf{a}(\mathbf{p}), \tag{4}$$

where ψ indicates the global phase offset, $\alpha_l \in \mathbb{R}$ is the amplitude of the l-th path (including LoS) and $d_l \in \mathbb{R}$ is the propagation distance [15]. The RIS phase profile vector at instant t is $\boldsymbol{\omega}_t \in \mathbb{C}^{M\times 1}$, and it can vary simultaneously with the BS downlink transmission. The RIS steering vector is described by $\mathbf{a}(\mathbf{q}) \in \mathbb{C}^{M\times 1}$, with m-th entry

$$[\mathbf{a}(\mathbf{q})]_m = e^{-j\frac{2\pi}{\lambda_c}(\|\mathbf{q}-\mathbf{p}_{\mathrm{RIS},m}\| - \|\mathbf{q}-\mathbf{p}_{\mathrm{RIS,\,ref}}\|)}, \tag{5}$$

where $\mathbf{q} \in \{\mathbf{p}, \mathbf{p}_{\mathrm{BS}}\}$ and $\mathbf{p}_{\mathrm{RIS,\,ref}}$ is the reference element's location. For the channel amplitude, we define the vector $\boldsymbol{\beta} \in \mathbb{R}_{>0}^{M\times 1}$ to describe the link between BS to UE via the RIS. The m-th entry of RIS's amplitude vector is modeled as [16]

$$[\boldsymbol{\beta}]_m = \frac{\sqrt{G}(\lambda_c/4)^2}{4\pi\|\mathbf{p}-\mathbf{p}_{\mathrm{RIS},m}\|\|\mathbf{p}_{\mathrm{BS}}-\mathbf{p}_{\mathrm{RIS},m}\|}, \tag{6}$$

where $G = G_{\mathrm{i},m}G_{\mathrm{r},m} \in \mathbb{R}$.

To separate the RIS link with LoS path and other multipath components, we can design the RIS phase profile so that it results in a balanced sequence, e.g., by $\boldsymbol{\omega}_t = -\boldsymbol{\omega}_{t+1}$, so that $h_{\mathrm{RIS},t} = -h_{\mathrm{RIS},t+1}$ for odd t and thus $\sum_{t=1}^{2T} h_{\mathrm{RIS},t} = 0$ [15]. By substituting the channel model in adjacent time instants so that $2h_{\mathrm{RIS},t} = (h_{\mathrm{LoS}}+h_{\mathrm{mp}}+h_{\mathrm{RIS},t}) - (h_{\mathrm{LoS}}+h_{\mathrm{mp}}+h_{\mathrm{RIS},t+1})$ and scaling the signal, we can express the final signal $\mathbf{y} \in \mathbb{C}^{T\times 1}$ of the RIS link as

$$\mathbf{y} = e^{j\psi}\mathbf{F}^\top(\boldsymbol{\beta} \odot \mathbf{a}(\mathbf{p})) + \mathbf{n}, \tag{7}$$

where $\mathbf{F} = [\mathbf{f}_1, ..., \mathbf{f}_T] \in \mathbb{C}^{M\times T}$ and $\mathbf{f}_\tau = \mathrm{diag}(\boldsymbol{\omega}_{2\tau-1})\mathbf{a}(\mathbf{p}_{\mathrm{BS}}) \in \mathbb{C}^{M\times 1}$, for $\tau \in [1, 2, ..., T]$. The added noise is $\mathbf{n} \sim \mathcal{CN}(\mathbf{0}, \rho\mathbf{I})$, where $\rho = N_0/(2E_s)$.

C. Problem Description

Our goal is to recover the UE position $\mathbf{p}$ in the presence of nuisance parameters $\boldsymbol{\beta}$ and ψ, from the received signal $\mathbf{y}$. This is challenging, as it generally involves $M+3$ real unknowns and $2T$ observations. Importantly, with $2T \ll M+3$, the problem is inherently unidentifiable. Next, we describe and propose a mismatched model to reduce the unknown parameters and estimate the user's location.

III. Mismatched Model, Estimator, and PEB

In this section, we first discuss the number of resolvable parameters $M+3$ in the estimation stage and propose mismatched models of $\mathbf{y}$ to estimate parameters accordingly. Then we derive the mismatched model's theoretical PEB.

A. Mismatched Model Specification

The true model (7) contains $M+3$ unknown parameters, which is usually larger than the pilot number $2T$ in most RIS-related research. Moreover, half of the pilots are used for canceling the LoS and multipath components. Thus, (7) presents a model with too many unknown parameters that cannot be

[1] Similar to [16], we assume RIS elements' gains are constant in all directions.

[2] In this work, we consider only the first-order bounces [14], [15], [17].

estimated from RIS's reflections. However, $\boldsymbol{\beta}$ may not vary significantly *within each RIS panel*, and we can break the whole structure evenly into multiple (virtual) sub-RISs that each has essentially a constant channel gain and decrease the number of unknowns. Hence, we model the whole RIS structure as comprising K virtual sub-RISs ($M \geq K \geq 1$), and the sub-RIS dependent channel gain vector is $\boldsymbol{b} = [b_1 \ldots, b_K]^\top \in \mathbb{R}_{>0}^{K\times 1}$, where b_k is the unknown channel amplitude of the k-th virtual sub-RIS, and the value of K is not related to the number of phase-coherent RIS panels. The mismatched model then becomes

$$\mathbf{y} \approx e^{j\psi}\mathbf{A}(\mathbf{p})\mathbf{b} + \mathbf{n}, \tag{8}$$

where

$$[\mathbf{A}(\mathbf{p})]_{[\tau,k]} = [\mathbf{F}^\top]_{[\tau,\frac{M(k-1)}{K}+1:\frac{Mk}{K}]}\mathbf{a}_k(\mathbf{p}) \in \mathbb{C} \tag{9}$$

$$\mathbf{a}_k(\mathbf{p}) = [\mathbf{a}(\mathbf{p})]_{[\frac{M(k-1)}{K}+1:\frac{Mk}{K}]} \in \mathbb{C}^{M/K\times 1}. \tag{10}$$

in which $\mathbf{a}_k(\mathbf{p})$ is the k-th sub-RIS's steering vector, and M/K is the element number of sub-RIS. Note that when $K = 1$, we have $\mathbf{A}(\mathbf{p}) = \mathbf{F}^\top\mathbf{a}(\mathbf{p})$ and $\mathbf{b}$ reverts to a scalar. Depending on the values of K, M, and T, we observe the following: (i) when $K + 3 \leq T$, it is feasible to estimate the mismatched model parameters; (ii) when $K + 3 > T$, the mismatched model parameters become unfeasible to estimate; (iii) when $K \to M$, the mismatched model approaches the true model and accurately describes the non-stationary RIS channel gain.

B. Proposed Mismatched Estimator

Assuming the condition $K + 3 < T$ holds, we can derive the associated loss function and maximum likelihood estimator as

$$\mathcal{L}(\mathbf{y}|\mathbf{b},\mathbf{p},\psi) = \|\mathbf{y} - e^{j\psi}\mathbf{A}(\mathbf{p})\mathbf{b}\|^2, \tag{11}$$

and

$$\widehat{\mathbf{b}},\widehat{\mathbf{p}},\widehat{\psi} = \arg\min_{\mathbf{b},\mathbf{p},\psi} \mathcal{L}(\mathbf{y}|\mathbf{b},\mathbf{p},\psi). \tag{12}$$

To solve (12), we first identify the stationary conditions for $\mathbf{b}(\mathbf{p})$ and $\psi(\mathbf{p})$ by setting the derivatives of the loss function with respect to these parameters to zero, yielding[3]

$$\psi(\mathbf{p}) = -\arg(\mathbf{y}^H\mathbf{A}(\mathbf{p})\mathbf{b}(\mathbf{p})), \tag{13}$$

$$\mathbf{b}(\mathbf{p}) = (\Re\{\mathbf{A}(\mathbf{p})^H\mathbf{A}(\mathbf{p})\})^{-1}\Re\{\mathbf{A}(\mathbf{p})^H e^{-j\psi}\mathbf{y}\}. \tag{14}$$

We observe that these two parameters are mutually dependent. To estimate the location $\mathbf{p}$, a grid search is necessary, where for each grid location $\mathbf{p}_g$, (13)–(14) are used to estimate $\psi(\mathbf{p}_g)$ and $\mathbf{b}(\mathbf{p}_g)$. Since these expressions are coupled, we break the dependency by initializing the estimate of ψ_{ini} with 0. The entire estimation method is outlined in Algorithm 1.

C. Mismatched Model-Based Lower Bound

Generally, the analytical lower bound of parameters of interest can be obtained by computing the corresponding Fisher information matrix (FIM) $\mathbf{J}_K(\boldsymbol{\eta}) \in \mathbb{R}^{(K+3)\times(K+3)}$ based on the mismatched model in (8). Hence, we start by calculating

[3]For $K = 1$, a further simplification is possible since the scalar b and $e^{j\psi}$ can be merged into a single complex unknown variable.

Algorithm 1 Proposed mismatched estimator

Initialize variables:
  $\mathbf{P}$: Area contains possible values for parameter $\mathbf{p}_g$.
  K: Number of virtual sub-RIS.
  γ: Iteration stopping threshold.
  I: Max iteration count to prevent infinite loops.
for each $\mathbf{p}_g$ in $\mathbf{P}$ **do**
  Compute $\mathbf{A}(\mathbf{p}_g)$
  Initialise $\psi_{\text{ini}}(\mathbf{p}_g) = 0$
  Set iteration index $i = 1$
  while $i \leq I$ **do**
    Update $\widehat{\mathbf{b}}_i(\mathbf{p}_g)$ via (14).
    $\delta_i(\mathbf{p}_g)$=$\|\mathbf{y} - e^{j\widehat{\psi}_i}\mathbf{A}(\mathbf{p}_g)\widehat{\mathbf{b}}_i\|^2$
    Compute $\widehat{\psi}_{i+1}(\mathbf{p}_g)$ via (13).
    if $i > 2$ **then**
      if $|\delta_i(\mathbf{p}_g) - \delta_{i-1}(\mathbf{p}_g)| \leq \gamma$ **then**
        Break
      end if
    end if
    $i = i + 1$
  end while
  $\delta(\mathbf{p}_g) = \delta_i(\mathbf{p}_g)$
end for
$\widehat{\mathbf{p}} = \arg\min_{\mathbf{p}_g} \delta(\mathbf{p}_g)$ and compute $\widehat{\mathbf{b}}_i(\widehat{\mathbf{p}})$ and $\widehat{\psi}_i(\widehat{\mathbf{p}})$.

$\mathbf{J}_K(\boldsymbol{\eta})$ of the noise-free signal $\boldsymbol{\mu} = \mathbf{y} - \mathbf{n}$ regarding the parameter vector $\boldsymbol{\eta} = [\mathbf{p}^\top, \boldsymbol{b}^\top, \psi]^\top \in \mathbb{R}^{(K+3)}$ as follows:

$$\mathbf{J}_K(\boldsymbol{\eta}) = \frac{2}{\rho}\Re\left\{\left(\frac{\partial\boldsymbol{\mu}}{\partial\boldsymbol{\eta}}\right)^H\frac{\partial\boldsymbol{\mu}}{\partial\boldsymbol{\eta}}\right\}, \tag{15}$$

where the derivatives are provided in the Appendix. As our estimation interest is the UE location, we first compute the inverse of the (15) and extract the submatrix regarding the location parameters, then we compute the trace and the square root of $[\mathbf{J}_K(\boldsymbol{\eta})^{-1}]_{[1:3,1:3]}$ to get $\text{PEB}_K(\mathbf{F},\boldsymbol{\eta})$ [18]. This yields

$$\text{PEB}_K(\mathbf{F},\boldsymbol{\eta}) = \sqrt{\text{Tr}([\mathbf{J}_K(\boldsymbol{\eta})^{-1}]_{[1:3,1:3]})}. \tag{16}$$

IV. Numerical Results

In this section, we present simulation-based numerical results to validate the model and assess the performance of the proposed method while also benchmarking against the prior-art method in [15].

A. Simulation Setup

The considered scenario has two 1-meter-long RIS panels equipped along two walls; each panel has 188 evenly deployed elements with half-wavelength spacing. More precisely, two RISs cover the linear region from the coordinate $[2,\ 0,\ 2]\,\text{m}$ to coordinate $[3,\ 0,\ 2]\,\text{m}$ and coordinate $[0,\ 2,\ 2]\,\text{m}$ to coordinate $[0,\ 3,\ 2]\,\text{m}$, respectively. The reference element's coordinate used for computing the steering vector in (5) is $\mathbf{p}_{\text{RIS, ref}} = [2,\ 0,\ 2]\,\text{m}$. For UE and BS locations, we assume $\mathbf{p}_{\text{UE}} = [4,\ 1,\ 1.8]\,\text{m}$ and $\mathbf{p}_{\text{BS}} = [5,\ 5,\ 2]\,\text{m}$. The gain factor G is set to $0\,\text{dB}$. The noise power spectral density N_0 is set to $-174\,\text{dBm/Hz}$ and bandwidth W equals $120\,\text{kHz}$. Such narrow bandwidth can reflect for example an individual subcarrier in OFDM-based systems. The random phase offset $\psi \in [0, \pi]$.

To evaluate the performance, we assess RMSEs with 1000 Monte Carlo simulations, and consider grid search over a $2\,\mathrm{m}$ by $2\,\mathrm{m}$ square region using x_{UE} and y_{UE} as the center coordinate. For simplicity, UE height z_{UE} is assumed known. We consider randomized codebook $\mathbf{F}$ while collect the averaged RMSEs and PEBs over ten independent instances of $\mathbf{F}$. While the received signal power among T observations is unequal, we vary the transmit power P_t and pilot number T in the evaluations to comprehensively assess the performance of the proposed method.

B. Reference Algorithm

For comparison purposes, we also simulate and evaluate the 'Direct Positioning (DP)' algorithm, described in [15], under the same model mismatch scenario. This reference method divides the entire RIS into K equal parts and assumes known channel gains for the RIS link at the receiver. The channel amplitudes for the elements of the k-th sub-RIS are set equal to b_k^{DP}, which is calculated from (6) by substituting $\mathbf{p}_{\mathrm{RIS},m}$ with the coordinates of the center element of the k-th sub-RIS. The estimated location is the point causing the minimum difference between the received signal with the expected signal. The corresponding estimator and PEB can be detailed as:

$$\widehat{\mathbf{p}}^{\mathrm{DP}} = \arg\min_{\mathbf{p},\psi} \sum_{\tau=1}^{T} \frac{|[\mathbf{y}]_\tau|^2}{\rho} \sin^2(\gamma_\tau), \tag{17a}$$

$$\gamma_\tau = \arg\big([\mathbf{y}]_\tau\big) - \arg\big([\mathbf{A}(\mathbf{p})]_{[\tau,1:K]}\mathbf{b}^{\mathrm{DP}}\big) - \psi, \tag{17b}$$

$$\mathrm{PEB}_K^{\mathrm{DP}} = \sqrt{\mathrm{Tr}\Big(\frac{\rho}{2}\Big[\Re\Big\{\Big(\frac{\partial \boldsymbol{\mu}^{\mathrm{DP}}}{\partial \mathbf{p}}\Big)^H \frac{\partial \boldsymbol{\mu}^{\mathrm{DP}}}{\partial \mathbf{p}}\Big\}^{-1}\Big]\Big)}. \tag{17c}$$

The intermediate parameter γ_τ measures the argument between the received signal $[\mathbf{y}]_\tau$ with the expectation. The vector $\mathbf{b}^{\mathrm{DP}} = [b_1^{\mathrm{DP}}, ..., b_K^{\mathrm{DP}}] \in \mathbb{R}_{>0}^{K\times 1}$ contains sub-RIS's channel amplitudes under the assumption of K sub-RISs. The noiseless signal is given by $\boldsymbol{\mu}_{\mathrm{DP}} = e^{j\psi}\mathbf{A}(\mathbf{p})\mathbf{b}_{\mathrm{DP}}$. Notably, the reference algorithm is subject to more optimistic PEB with perfect knowledge of the channel amplitude $\mathbf{b}^{\mathrm{DP}}$ and phase offset ψ.

C. Results and Discussion

1) Channel Non-Stationarity Estimation: We begin by examining the estimated channel non-stationarity. Fig. 2 illustrates the estimated channel amplitudes for different numbers of sub-RISs (K). We set T to 64, P_t to $25\,\mathrm{dBm}$, and consider a random realization or instance of $\mathbf{F}$. The blue dashed line presents the ground truth of channel amplitude ($\boldsymbol{\beta}$). We can observe a significant decrease in the ground-truth channel amplitudes for the first 188 RIS elements, which range between $-71\,\mathrm{dB}$ and $-74\,\mathrm{dB}$. The channel amplitudes for the second RIS panel elements have, in turn, more insignificant variations and remain close to $-77\,\mathrm{dB}$. Then, we show the estimated $\widehat{\mathbf{b}}$ for sub-RISs with four values of K. When $K = 1$, the estimated value approximates the average channel amplitude across all elements. As K increases, the estimated amplitudes get closer to the ground truth, but performance is limited by the column number (T) of $\mathbf{F}$. This is evident in the purple line ($K = 47$) with larger variations compared to the ground truth, as K is already close to T.

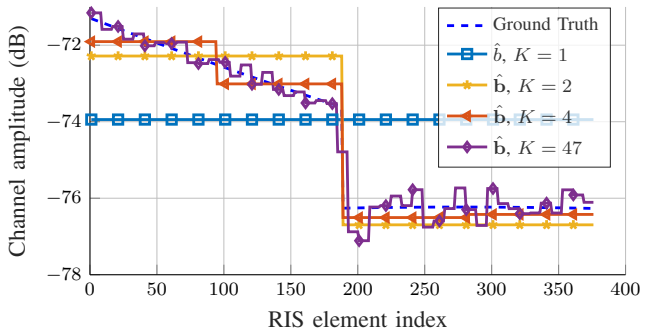

Fig. 2. True channel amplitudes and the estimated channel amplitudes for K sub-RISs ($K \in \{1, 2, 4, 47\}$) with $T = 64$ and $P_t = 25\,\mathrm{dBm}$.

2) Performance Evaluation with Transmission Power P_t: To evaluate the impact of transmission power on performance, we next fix the number of pilots $T = 64$ and vary P_t from $0\,\mathrm{dBm}$ to $35\,\mathrm{dBm}$. Fig. 3 presents the RMSE and PEB curves for the two methods, depicted with solid and dashed lines. In the proposed method context, the PEB quantifies the achievable localization accuracy of any unbiased estimator, while RMSE encompasses both noise-induced estimation errors and bias arising from the model mismatch. With higher values of P_t, the bias becomes the dominant factor affecting RMSE. Employing a mismatched model with a higher value of K helps to reduce this bias, thereby narrowing the gap between the RMSE and the PEB. Biased estimators are generally known to sometimes result in a smaller RMSE compared to unbiased estimators [19]. Consequently, the RMSE curves for the proposed method occasionally fall slightly below the PEB. For the DP reference method, the two RMSE curves are represented by green and black solid lines. The RMSE for $K = 4$ at $P_t = 35\,\mathrm{dBm}$ shows better accuracy and closer alignment with the corresponding PEB than that of $K = 1$. Since the PEB of DP is the optimistic lower bound with known channel amplitude and phase, the PEB curves of the reference algorithm are lower than those of the proposed method. We can observe that at higher P_t range, both methods with $K = 4$ show comparable performance, while the proposed method offers clearly increased resilience in the important range of lower P_t values, compared to the DP method, demonstrating its ability to maintain centimeter scale or better accuracy in noisy environments.

3) Performance Evaluation with Pilot Number T: Given that the proposed method requires $K + 3 < T$ to estimate all unknowns, and that Fig. 2 already indicated inaccurate estimation when $K + 3$ is close to T, the number of pilots is one important parameter controlling the proposed method's performance. To assess this, we provide Monte Carlo simulations with $P_t = 25\,\mathrm{dBm}$, while varying the number of T from 10 to 100 – with the results shown in Fig. 4. At such higher P_t value, both methods with $K = 1$ show sensitivity to changes in T, where increasing the pilot number will significantly enhance the performance. However, with the assumption of $K = 4$, two methods work accurately across all T values. The results show that the proposed method – despite operating under more realistic and challenging assumptions – performs as well as the reference work even with $T = 10$. Furthermore, the

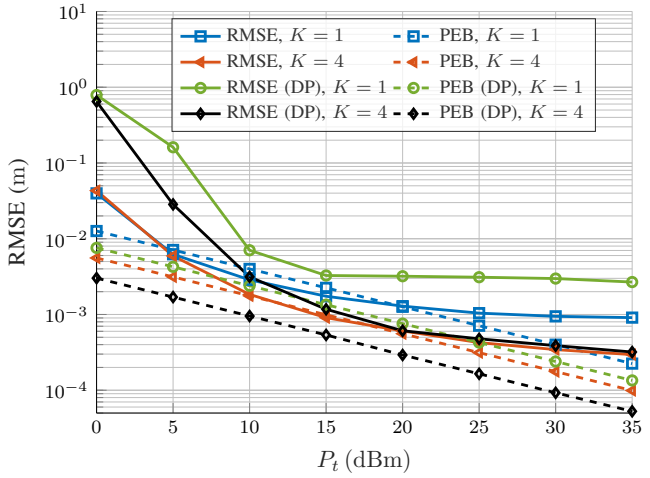

Fig. 3. RMSE and PEB curves of the proposed method and the reference algorithm (DP) for fixed $T = 64$ and varying P_t.

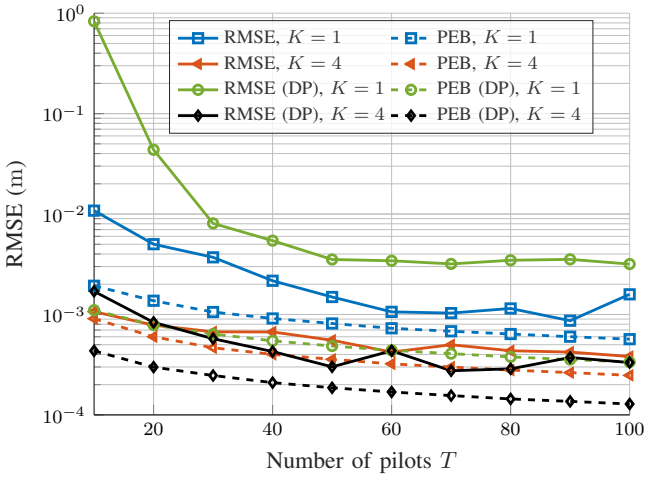

Fig. 4. RMSE and PEB curves of the proposed method and the reference method DP for fixed P_t of 25 dBm while varying T.

mismatched model-based estimator, which reduces the number of unknowns from $M+3$ to $K+3$, eases the requirement of T, thus proving the localization capability by using limited pilots. The selection of an optimal K under the constraint of T deserves further exploration, forming a topic for future work.

V. Conclusion

In this paper, we proposed and described a novel UE localization method in the near-field region of RISs, addressing the estimation challenge of channel non-stationarity over RIS elements. Our approach utilizes a flexible mismatched model to approximate the true signal model and develops an iterative localization method that accounts for the RIS channel non-stationarity. This allows for locating the user without requiring physical decomposition of the RIS and the knowledge of element-wise channel amplitudes. The Monte Carlo simulations using a narrowband signal at 28 GHz demonstrate the estimator's accuracy by comparing RMSE and PEB against the prior-art reference algorithm. While the current evaluations assumed the knowledge of the UE's height and also involved only two RIS panels, our approach can be extended to 3D localization and more advanced RIS deployment scenarios.

Appendix

Corresponding to unknown parameters $\mathbf{p}$, $\boldsymbol{b}$ and ψ, the partial derivatives of (15) can be expressed as follows:

$$\frac{\partial \boldsymbol{\mu}}{\partial \mathbf{p}} = e^{j\psi}[\mathbf{F}^{\top}]_{[1:T,\frac{M(k-1)}{K}+1:\frac{Mk}{K}]}\frac{[\partial \mathbf{a}(\mathbf{p})]_{[\frac{M(k-1)+K}{K}+1:\frac{Mk}{K}]}}{\partial \mathbf{p}}\mathbf{b}, \tag{18}$$

in which $[\partial \mathbf{a}(\mathbf{p})]_m/\partial x_{\text{UE}} = -j2\pi[\mathbf{a}(\mathbf{p})]_m\eta(m, x_{\text{UE}})/\lambda_c$, $\partial\boldsymbol{\mu}/\partial[\boldsymbol{b}]_k = e^{j\psi}\mathbf{A}(\mathbf{p})\mathbf{v}$, and $\partial\boldsymbol{\mu}/\partial\psi = je^{j\psi}\mathbf{A}(\mathbf{p})\mathbf{b}$, where $\eta(m, x_{\text{UE}}) = (x_{\text{UE}} - x_{\text{RIS},m})/\|\mathbf{p} - \mathbf{p}_{\text{RIS},m}\| - (x_{\text{UE}} - x_{\text{RIS, ref}})/\|\mathbf{p} - \mathbf{p}_{\text{RIS, ref}}\|$ and the k-th element of $\mathbf{v} \in \mathbb{R}^{K\times 1}$ is 1 while the rest are zeros.

References

[1] C. J. Bernardos and M. A. Uusitalo, "European vision for the 6G network ecosystem," *The 5G Infrastructure Association*, 2021.

[2] F. Wen and H. Wymeersch, "5G synchronization, positioning, and mapping from diffuse multipath," *IEEE Wireless Communications Letters*, vol. 10, no. 1, pp. 43–47, Jan. 2021.

[3] M. Ahmed *et al.*, "A survey on STAR-RIS: Use cases, recent advances, and future research challenges," *IEEE Internet of Things Journal*, pp. 14 689–14 711, Aug. 2023.

[4] C. Huang *et al.*, "Reconfigurable intelligent surfaces for energy efficiency in wireless communication," *IEEE Transactions on Wireless Communications*, vol. 18, no. 8, pp. 4157–4170, Aug. 2019.

[5] M. He *et al.*, "RIS-assisted quasi-static broad coverage for wideband mmwave massive MIMO systems," *IEEE Transactions on Wireless Communications*, vol. 22, no. 4, pp. 2551–2565, Apr. 2023.

[6] J. Hu *et al.*, "Metasketch: Wireless semantic segmentation by reconfigurable intelligent surfaces," *IEEE Transactions on Wireless Communications*, vol. 21, no. 8, pp. 5916–5929, Aug. 2022.

[7] E. Björnson, Ö. T. Demir, and L. Sanguinetti, "A primer on near-field beamforming for arrays and reconfigurable intelligent surfaces," in *Proc. IEEE Asilomar Conference on Signals, Systems, and Computers*, Oct. 2021, pp. 105–112.

[8] M. Cui *et al.*, "Near-field MIMO communications for 6G: Fundamentals, challenges, potentials, and future directions," *IEEE Communications Magazine*, vol. 61, no. 1, pp. 40–46, Jan. 2023.

[9] X. Zhang and H. Zhang, "Hybrid reconfigurable intelligent surfaces-assisted near-field localization," *IEEE Communications Letters*, vol. 27, no. 1, pp. 135–139, Jan. 2023.

[10] R. Ghazalian *et al.*, "Joint 3D user and 6D hybrid reconfigurable intelligent surface localization," Jan. 2024, arXiv:2401.03852.

[11] M. Rahal *et al.*, "Constrained RIS phase profile optimization and time sharing for near-field localization," in *Proc. IEEE Vehicular Technology Conference (VTC 2022 Spring)*, Jun. 2022, pp. 1–6.

[12] Z. Abu-Shaban *et al.*, "Near-field localization with a reconfigurable intelligent surface acting as lens," in *Proc. IEEE International Conference on Communications (ICC 2021)*, Jun. 2021, pp. 1–6.

[13] Y. Pan *et al.*, "RIS-aided near-field localization and channel estimation for the terahertz system," *IEEE Journal of Selected Topics in Signal Processing*, vol. 17, no. 4, pp. 878–892, Jul. 2023.

[14] S. Huang *et al.*, "Near-field RSS-based localization algorithms using reconfigurable intelligent surface," *IEEE Sensors Journal*, vol. 22, no. 4, pp. 3493–3505, Feb. 2022.

[15] D. Dardari *et al.*, "LOS/NLOS near-field localization with a large reconfigurable intelligent surface," *IEEE Transactions on Wireless Communications*, vol. 21, no. 6, pp. 4282–4294, Jun. 2022.

[16] E. Björnson *et al.*, "Reconfigurable intelligent surfaces: A signal processing perspective with wireless applications," *IEEE Signal Processing Magazine*, vol. 39, no. 2, pp. 135–158, Mar. 2022.

[17] X. Zhang and H. Zhang, "Hybrid reconfigurable intelligent surfaces-assisted near-field localization," *IEEE Communications Letters*, vol. 27, no. 1, pp. 135–139, Jan. 2023.

[18] S. Sand, A. Dammann, and C. Mensing, *Positioning in Wireless Communication Systems*. John Wiley and Sons Inc, 2014.

[19] C. M. Bishop, *Pattern Recognition and Machine Learning*. New York: Springer Publishing Company, 2006.